Eur. Phys. J. C (2019) 79:619
https://doi.org/10.1140/epjc/s10052-019-7099-3

THE EUROPEAN PHYSICAL JOURNAL C

Regular Article - Theoretical Physics

Transverse expansion of hot magnetized Bjorken flow in heavy ion collisions

Mohsen Haddadi Moghaddam[1,2], **B. Azadegan**[1], **A. F. Kord**[1,a], **W. M. Alberico**[2]

[1] Department of Physics, Hakim Sabzevari University (HSU), P.O.Box 397, Sabzevar, Iran
[2] Department of Physics, University of Turin and INFN, Turin, Via P. Giuria 1, 10125 Turin, Italy

Received: 1 January 2019 / Accepted: 2 July 2019 / Published online: 22 July 2019

Abstract We argue that the existence of an inhomogeneous external magnetic field can lead to radial flow in transverse plane. Our aim is to show how the introduction of a magnetic field generalizes the Bjorken flow. We investigate the effect of an inhomogeneous weak external magnetic field on the transverse expansion of in-viscid fluid created in high energy nuclear collisions. In order to simplify our calculation and compare with Gubser model, we consider the fluid under investigation to be produced in central collisions, at small impact parameter; azimuthal symmetry has been considered. In our model, we assume an inhomogeneous external magnetic field following the power-law decay in proper time and having radial inhomogeneity perpendicular to the radial velocity of the in-viscid fluid in the transverse plane; then the space time evolution of the transverse expansion of the fluid is obtained. We also show how the existence of an inhomogeneous external magnetic field modifies the energy density. Finally we use the solutions for the transverse velocity and energy density in the presence of a weak magnetic field, to estimate the transverse momentum spectrum of protons and pions emerging from the Magneto-hydrodynamic solutions.

1 Introduction

Collisions of two heavy nuclei at high energy produce a hot and dense fireball. Quarks and gluons could reach the deconfined state, called quark gluon plasma (QGP), in a very short time (∼1 fm/c) after the initial hard parton collisions of nuclei. A very handy model which describes the typical motion of partons after collision is the Bjorken flow model [1]. Based on some assumptions such as boost invariance along beam line, translation and rotation invariance in the transverse plane, one can show that all quantities of interest only depend on the proper time τ and not on the transverse $(x_\perp, \phi)$ coordinates, nor on the rapidity η. Using the above assumptions, together with invariance under reflection $\eta \to -\eta$, one can determine the four-velocity profile. The four-velocity is $u^\mu = (1, 0, 0, 0)$ in the $(\tau, x_\perp, \phi, \eta)$ coordinate system. Besides, it is straightforward to show that the energy density decays as $\tau^{-4/3}$ in the local rest frame if the medium is equilibrated and the equation of state of the medium is $p = \epsilon/3$.

Based on the size of the colliding nuclei, one realizes that assuming translational invariance in the transverse plane is not realistic [2]. Using the Bjorken model one often assumes that in medium the radial flow ($u_\perp$) is zero. However, this assumption is not correct even for central collisions, and it might mislead the subsequent hydrodynamical flow, on which much of heavy-ions phenomenology depends.

The aim of our work is to generalize the Bjorken model by considering an inhomogeneous external magnetic field acting on the medium. We show that the presence of the magnetic field leads to non-zero radial flow. In order to simplify our calculation, we consider central heavy ions collisions. We still consider rotational symmetry around beam line, as well as boost invariance along the beam line. However, we assume that translational invariance in the transverse plane is broken by the magnetic field. Then we obtain a four-velocity profile which has a non zero radial component. In the present study for central collisions (small impact parameter), we provide an analytical solution for the transverse expansion of a hot magnetized plasma, based on perturbation theory.

We concentrate on the special case of a $(1 + 2)$ dimensional, longitudinally boost-invariant fluid expansion as the Bjorken flow; the fluid also radially expands in the transverse plane, under the influence of an inhomogeneous external magnetic field which is transverse to the radial fluid velocity (this proceeds according to the so called *transverse* MHD).

We consider an inviscid fluid coupled to an external magnetic field. As one expects in central collisions, we assume that the external magnetic fields is small compared to the

[a] e-mail: afarzaneh@hsu.ac.ir

fluid energy density [3]. Therefore, we can neglect the coupling to the Maxwell's equations and solve the conservation equations perturbatively and analytically [4].

Moreover the presence of external magnetic field may induce internal electromagnetic fields of the fluid. The internal magnetic fields are dictated by Maxwell's equations and one should solve the conservation equations and Maxwell's equations coupled to each other by numerical methods [25]. In this work we neglect the effects of such internal magnetic field. Hence we will consider the system with an inhomogeneous external magnetic field and will investigate the anisotropic transverse flow and the modified energy density of the fluid induced by the external magnetic fields. As in Gubser flow, the finite size of the colliding nuclei leads to non-zero radial velocity ($u_\perp$); we show that the inhomogeneous weak external magnetic field also leads to nonzero radial velocity and can produce modifications on the radial expansion of the plasma in central collisions.

We remind the reader that recently a wide range of studies has shown that relativistic heavy-ion collisions create also huge magnetic field due to the relativistic motion of the colliding heavy ions carrying large positive electric charge [5–16]. The interplay of magnetic field and QGP matter has been predicted to lead to a number of interesting phenomena. One can see recent reviews on this topic in Refs. [17–20] for more details.

Previous theoretical studies show that the strength of the produced magnetic field depends on the center of mass energy ($\sqrt{s_{NN}}$) of the colliding nuclei, on the impact parameter (b) of the collision, on the electrical and chiral conductivities (σ_{el}, σ_χ) of the medium [6,10,11,15]. Moreover, the magnetic field in central collisions becomes non-zero due to the fluctuating proton position from event to event [3,13]. It has been found that the ratio of magnetic field energy to the fluid energy density ($\sigma = eB^2/2\epsilon$) in central collisions is much smaller than in peripheral collisions [3]. The authors of Ref. [3] computed the fluid energy density and electromagnetic field by using the Monte Carlo Glauber model. The initial energy density for the fluid at proper time $\tau_i = 0.5$ fm was fixed to $\sim$40 GeV/fm^3. They found $\sigma \ll 1$ for most of the events, at the center of the collision zone and for impact parameter $b = 0$, while for large b as compared to central collisions, σ becomes larger as a result of the increase in magnetic field and decrease in fluid energy density. In a plasma $\sigma = 1$ indicates that the effect of magnetic field in the plasma evolution can not be neglected, but it is worth observing that in some situations, even $\sigma \sim 0.01$ may affect the hydrodynamical evolution [3].

Recently, some efforts in numerical and analytical works have been made, based on the relativistic magnetohydrodynamic (RMHD) setup, to describe high energy heavy ion collisions (see, for example, [4] and [21–30]). In [4] the goal was to obtain an analytical solution in $(1 + 1)$ dimensional Bjorken flow for ideal transverse RMHD, and the conservation equations were solved perturbatively and analytically. In our previous work [25], we developed a simple code for transverse expansion in (1+1D) RMHD setup in order to solve coupled conservation equations and Maxwell's equations numerically.

We found that this coupling can indeed affect the solutions with respect to the ones of Ref. [4]. In the present work, we show that the perturbative approach of Ref. [4] can be applied to the case of central collision, in order to find analytical solution for the transverse expansion of QGP matter in the presence of an external magnetic field.

The paper is organized as follows. In Sect. 2, we introduce the ideal relativistic magnetohydrodynamic equations in their most general form, considering them in the case of a plasma with infinite electrical conductivity. In Sect. 3 we present our perturbative approach and the analytical solutions we found. Section 4 illustrates and discusses the general results obtained. Section 5 contains a calculation of the transverse momentum spectrum together with a comparison of this quantity with experimental results obtained at RHIC. Conclusions and subsequent outlook can be found in the last section.

2 Ideal relativistic magneto-hydrodynamic

We deal with the case of an ideal non-resistive plasma, with vanishing electric field in the local rest-frame ($e^\mu = 0$), which is embedded in an external magnetic field (b_μ) [31,32]. The energy momentum conservation equations read:

$$d_\mu (T^{\mu\nu}_{pl} + T^{\mu\nu}_{em}) = 0, \tag{1}$$

where

$$T^{\mu\nu}_{pl} = (\epsilon + P)u^\mu u^\nu + P g^{\mu\nu} \tag{2}$$

$$T^{\mu\nu}_{em} = b^2 u^\mu u^\nu + \frac{1}{2} b^2 g^{\mu\nu} - b^\mu b^\nu. \tag{3}$$

In the above $g_{\mu\nu}$ is the metric tensor, ϵ and P are the energy density and pressure, respectively. Moreover d_μ is the covariant derivative, defined later in Eq. (9).

The four velocity is defined as

$$u_\mu = \gamma(1, \vec{v}), \ \gamma = \frac{1}{\sqrt{1 - v^2}}$$

satisfying the condition $u^\mu u_\mu = -1$.

Canonically one takes projections of the equation $d_\mu(T^{\mu\nu}_{pl} + T^{\mu\nu}_{em}) = 0$ along the parallel and perpendicular directions to u_ν. The parallel projection is obtained via $u_\nu d_\mu(T^{\mu\nu}_{pl} + T^{\mu\nu}_{em})$, which gives:

$$D(\epsilon + b^2/2) + (\epsilon + P + b^2)\Theta + u_\nu b^\mu (d_\mu b^\nu) = 0, \tag{4}$$

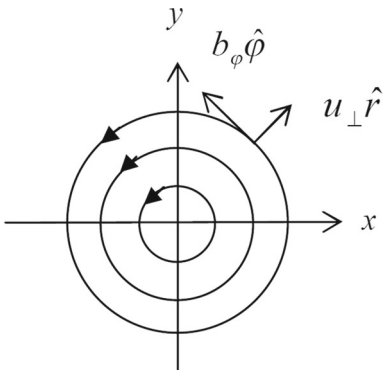

Fig. 1 Transverse MHD $\mathbf{u}\cdot\mathbf{B}=0$

For the transverse projection we use the definition $\Delta^{\mu\nu}=g^{\mu\nu}+u^\mu u^\nu$; then $\Delta^\alpha_\nu d_\mu(T^{\mu\nu}_{pl}+T^{\mu\nu}_{em})=0$ gives:

$$(\epsilon+P+b^2)Du^\alpha=-\nabla^\alpha\left(P+\frac{1}{2}b^2\right)+d_\mu(b^\mu b^\alpha)+u^\alpha u_\nu d_\mu(b^\mu b^\nu). \tag{5}$$

Notice that α should be a spacelike index. Moreover

$$D=u^\mu d_\mu,\quad ,\Theta=d_\mu u^\mu,\quad ,\nabla^\alpha=\Delta^\alpha_\nu d^\nu. \tag{6}$$

3 Ideal transverse MHD setup in the transverse expansion

We assume that the medium has a finite transverse size and expands both radially and along the beam axis, the only nonzero components of $u_\mu=(u_\tau,u_\perp,0,0)$ being u_τ, which describes the boost invariant longitudinal expansion, and $u_\perp$, which describes the transverse expansion. For the sake of simplicity we suppose that $u_\phi=0$ because we claimed that the system is rotationally symmetric.

It is more convenient to work in Milne coordinates, $x^m=(\tau,x_\perp,\phi,\eta)$, such that:

$$\begin{aligned}&x=x_\perp\cos\phi,\ y=x_\perp\sin\phi,\\&z=\tau\sinh\eta,t=\tau\cosh\eta,\\&\tau=\sqrt{t^2-z^2},\ \eta=\frac{1}{2}\ln\frac{t+z}{t-z},\\&\phi=\tan^{-1}(y/x),\ x_\perp^2=x^2+y^2\end{aligned} \tag{7}$$

Moreover we suppose that the external magnetic field is located in the transverse plane as $b_\mu=(0,0,b_\phi,0)$ where $b^\mu b_\mu\equiv b^2$ is defined. Our setup is depicted in Fig. 1. The metric for the coordinates $(\tau,x_\perp,\phi,\eta)$ is parameterized as follows: $g_{\mu\nu}=diag(-1,1,x_\perp^2,\tau^2)$ and $g^{\mu\nu}=diag(-1,1,1/x_\perp^2,1/\tau^2)$. Correspondingly

$$ds^2=-d\tau^2+dx_\perp^2+x_\perp^2d\phi^2+\tau^2d\eta^2. \tag{8}$$

In this configuration it is found that $u^\tau=-u_\tau=-u_0$ and $\partial^\tau=-\partial_\tau$.

We have to take care of the following covariant derivative (instead of the usual one):

$$d_\mu A^\mu=\partial_\mu A^\mu+\Gamma^\mu_{\mu\rho}A^\rho, \tag{9}$$

where the Cristoffel symbols are defined as follows:

$$\Gamma^i_{jk}=\frac{1}{2}g^{im}\left(\frac{\partial g_{mj}}{\partial x^k}+\frac{\partial g_{mk}}{\partial x^j}-\frac{\partial g_{jk}}{\partial x^m}\right). \tag{10}$$

Here we frequently take advantage of the following formula:

$$\Gamma^i_{jk}=0,\ for\ i\neq j\neq k \tag{11}$$

$$\Gamma^i_{jj}=-\frac{1}{2g_{ii}}\frac{\partial g_{jj}}{\partial x^i},\ for\ i\neq j \tag{12}$$

$$\Gamma^i_{ij}=\Gamma^i_{ji}=\frac{1}{2g_{ii}}\frac{\partial g_{ii}}{\partial x^j}=\frac{1}{2}\frac{\partial\ln g_{ii}}{\partial x^j}. \tag{13}$$

Hence the only non-zero Christoffel symbols, here, are $\Gamma^\tau_{\eta\eta}=\tau$, $\Gamma^{x_\perp}_{\phi\phi}=-x_\perp$, $\Gamma^\phi_{x_\perp\phi}=\frac{1}{x_\perp}$, $\Gamma^\eta_{\tau\eta}=\frac{1}{\tau}$. Now D and Θ are given by:

$$D=-u_0\partial_\tau+u_\perp\partial_\perp,\ \Theta=-\partial_\tau u_0+\frac{u_\perp}{x_\perp}+\frac{\partial u_\perp}{\partial x_\perp}-\frac{u_0}{\tau}. \tag{14}$$

The constraint $u^2=u^\tau u_\tau+u^\perp u_\perp=-u_0^2+u_\perp^2=-1$ must be satisfied as well.

We now look for the perturbative solution of the conservation equations in the presence of a weak external inhomogeneous magnetic field pointing along the ϕ direction in an inviscid fluid with infinite electrical conductivity and obeying Bjorken flow in z - direction. Our setup is given by:

$$b_\mu=(0,0,\lambda b_\phi,0),\ u_\mu=(1,\lambda^2u_\perp,0,0), \tag{15}$$

$$\epsilon=\epsilon_0(\tau)+\lambda^2\epsilon_1(\tau,x_\perp),\ \epsilon_0(\tau)=\frac{\epsilon_c}{\tau^{4/3}}, \tag{16}$$

where ϵ_c is the energy density at proper time τ_0. Then the energy conservation and Euler equations [Eqs. (4), (5)] reduce to two coupled differential equations. Up to $O(\lambda^2)$, they are:

$$\partial_\tau\epsilon_1-\frac{4\epsilon_c}{3\tau^{4/3}}\left(\frac{u_\perp}{x_\perp}+\frac{\partial u_\perp}{\partial x_\perp}\right)+\frac{4\epsilon_1}{3\tau}+b_\phi\partial_\tau b_\phi+\frac{b_\phi^2}{\tau}=0 \tag{17}$$

$$\partial_\perp\epsilon_1-\frac{4\epsilon_c}{\tau^{4/3}}\partial_\tau u_\perp+\frac{4\epsilon_c}{3\tau^{7/3}}u_\perp+3b_\phi\partial_\perp b_\phi+\frac{3b_\phi^2}{x_\perp}=0. \tag{18}$$

The combination of the two above equations yields a partial differential equation depending on $u_\perp$ and b_ϕ:

$$u_\perp - \tau^2\partial_\perp\left(\frac{u_\perp}{x_\perp}\right) - \tau^2\partial_\perp^2 u_\perp - \tau\partial_\tau u_\perp + 3\tau^2\partial_\tau^2 u_\perp - \frac{3\tau^{7/3}}{x_\perp\epsilon_c}b_\phi^2 - \frac{3\tau^{7/3}}{4\epsilon_c}\partial_\perp b_\phi^2 - \frac{9\tau^{10/3}}{4x_\perp\epsilon_c}\partial_\tau b_\phi^2 - \frac{3\tau^{10/3}}{4\epsilon_c}\partial_\perp\partial_\tau b_\phi^2 = 0. \tag{19}$$

For $b_\phi = 0$, Eq. (19) is a homogeneous partial differential equation, which can be solved by separation of variables. The general solution is

$$u_\perp^h(\tau, x_\perp) = \sum_k (c_1^k J_1(kx_\perp) + c_2^k Y_1(kx_\perp)) \times (c_1'^k \tau^{2/3} J_{1/3}(k\tau/\sqrt{3}) + c_2'^k \tau^{2/3} Y_{1/3}(k\tau/\sqrt{3})), \tag{20}$$

where k can be real or imaginary numbers, $c_{1,2}^k$ and $c_{1,2}'^k$ are integration constants.

For non-vanishing b_ϕ we assume a space-time profile of the magnetic field in central collisions in the form:

$$b_\phi^2(\tau, x_\perp) = B_c^2 \tau^n \sqrt{\alpha} x_\perp e^{-\alpha x_\perp^2}. \tag{21}$$

We see that the magnitude of b_ϕ is zero at $x_\perp = 0$. In order to find solutions for transverse velocity $u_\perp$ and energy density ϵ consistently with the assumed magnetic field, we found it convenient to first expand the magnetic field, Eq. (21) into a series of $x_\perp$-dependent functions:

$$b_\phi^2(\tau, x_\perp) = \sum_k \tau^n B_k^2 \, f(kx_\perp), \tag{22}$$

where $k \geq 1$ are now real integers and B_k^2 are constants. For simplicity, we have assumed the time dependence of the magnetic field square as τ^n with $n < 0$, which approximately characterizes the decay of the magnetic field in heavy ion collisions. This is our key to convert the solution of the partial differential Eq. (19) into a summation of solutions of ordinary differential equations.

Moreover we replace the solution (20) for the radial velocity $u_\perp(\tau, x_\perp)$, which is valid for $b_\phi = 0$, with the following Ansatz [4]:

$$u_\perp(\tau, x_\perp) = \sum_k \Big(a_k(\tau) J_1(kx_\perp) + b_k(\tau) Y_1(kx_\perp)\Big). \tag{23}$$

It mantains the $x_\perp$ dependence of Eq. (20), but embodies the τ dependence in the coefficients of the Bessel functions. Note that from the initial condition $u_\perp(\tau, x_\perp = 0) = 0$ it follows that $b_k(\tau) = 0$.

Now we can substitute the Eqs. (22) and (23) into Eq. (19) and end up with the equation (at fixed k):

$$J_1(kx_\perp)(1 + \tau^2k^2 - \tau\partial_\tau + 3\tau^2\partial_\tau^2)a_k(\tau) - \frac{3\tau^{7/3+n}}{4\epsilon_c}B_k^2\left(\frac{f(x_\perp)}{x_\perp}(4+3n) + \partial_\perp(f(x_\perp))k(1+n)\right) = 0. \tag{24}$$

Here we can apply separation of variables, thus obtaining the following ordinary differential equation for the function $f(kx_\perp)$:

$$(1+n)kx_\perp\partial_\perp f(kx_\perp) + (4+3n)f(kx_\perp) = kx_\perp J_1(kx_\perp). \tag{25}$$

Its general solution is given by

$$f(kx_\perp) = \frac{k^2x_\perp^2\Gamma\left(\frac{2nk+2k+3n+4}{2nk+2k}\right){}_1F_2\left(\frac{2nk+2k+3n+4}{2nk+2k}; 2, \frac{4nk+4k+3n+4}{2nk+2k}; -\frac{1}{4}k^2x_\perp^2\right)}{4(n+1)\Gamma\left(\frac{4kn+4k+3n+4}{2kn+2k}\right)} + d_1(k^2(n+1)x_\perp)^{-\frac{3n+4}{kn+k}}, \tag{26}$$

where ${}_1F_2$ is the hypergeometric function. The first term is a well-defined function, but the second one diverges in $x_\perp = 0$ for any n except $n = -4/3$ which will be considered in details; hence, d_1 must be zero. For two values of the parameter n, $n = -1$ and $n = -4/3$, the solution of Eq. (25) takes a simple form:

$$f(kx_\perp) = kx_\perp J_1(kx_\perp) \quad (\text{for } n = -1) \tag{27}$$

and

$$f(kx_\perp) = d_2 + 3J_0(kx_\perp) \quad (\text{for } n = -4/3). \tag{28}$$

In order to implement the orthogonal properties of the Bessel functions, for the case $n = -4/3$ we set $d_2 = 0$ in Eq. (28). Then we can easily describe the external magnetic field as a series of Bessel functions, by restricting ourselves to the cases $n = -1$ and $n = -4/3$.

We write the solution for $n = -1$ as

$$b_\phi^2(\tau, x_\perp) = \sum_k \tau^{-1} B_k^2 \, \beta_{1k}\frac{x_\perp}{a} \, J_1\left(\beta_{1k}\frac{x_\perp}{a}\right) \tag{29}$$

where the coefficients B_k^2 are given by

$$B_k^2 = \frac{2a}{a^2\beta_{1k}[J_2(\beta_{1k})]^2}\int_0^a J_1\left(\beta_{1k}\frac{x_\perp}{a}\right) b_\phi^2 \, dx_\perp, \tag{30}$$

β_{1k} being the kth zero of J_1.

For $n = -4/3$ the solution for the magnetic field can be written as

$$b_\phi^2(\tau, x_\perp) = \sum_k \tau^{-4/3} B_k^2 \, 3 \, J_0\left(\beta_{0k}\frac{x_\perp}{a}\right) \tag{31}$$

where the coefficients B_k^2 are given by

$$B_k^2 = \frac{2}{3\,a^2[J_1(\beta_{0k})]^2}\int_0^a x_\perp J_0\left(\beta_{0k}\frac{x_\perp}{a}\right) b_\phi^2 \, dx_\perp \tag{32}$$

β_{0k} being the kth zero of J_0; in the above $k = \beta_{ik}/a$ ($i = 0, 1$).

Finally the coefficients $a_k(\tau)$ in Eq. (23) can be obtained by solving the following ordinary differential equation:

$$\left(k^2\tau^2+1\right) a_k(\tau)+\tau\left(3\tau a_k''(\tau)-a_k'(\tau)\right)-\frac{3kB_k^2\tau^{n+\frac{7}{3}}}{4\epsilon_c}=0. \tag{33}$$

The analytical solution for $n = -1$ is

$$\begin{aligned} a_k(\tau) &= c_1^k\tau^{2/3}J_{\frac{1}{3}}\left(\frac{k\tau}{\sqrt{3}}\right)+c_2^k\tau^{2/3}Y_{\frac{1}{3}}\left(\frac{k\tau}{\sqrt{3}}\right)\\ &+\frac{\pi kB_k^2}{48\Gamma\left(\frac{2}{3}\right)\Gamma\left(\frac{7}{6}\right)\Gamma\left(\frac{4}{3}\right)\epsilon_c\sqrt[3]{k\tau}}\\ &\times\left(-2^{2/3}\sqrt[3]{3}\tau^{4/3}\Gamma\left(\frac{2}{3}\right)\Gamma\left(\frac{7}{6}\right)(k\tau)^{2/3}J_{\frac{1}{3}}\right.\\ &\times\left(\frac{k\tau}{\sqrt{3}}\right){}_1F_2\left(\frac{1}{2};\frac{4}{3},\frac{3}{2};-\frac{1}{12}k^2\tau^2\right)\\ &+2\sqrt[3]{2}3^{2/3}\tau^{4/3}\Gamma\left(\frac{4}{3}\right)\Gamma\left(\frac{1}{6}\right)J_{\frac{1}{3}}\\ &\times\left(\frac{k\tau}{\sqrt{3}}\right){}_1F_2\left(\frac{1}{6};\frac{2}{3},\frac{7}{6};-\frac{1}{12}k^2\tau^2\right)\\ &+2^{2/3}3^{5/6}\tau^{4/3}\Gamma\left(\frac{2}{3}\right)\Gamma\left(\frac{7}{6}\right)(k\tau)^{2/3}Y_{\frac{1}{3}}\\ &\times\left.\left(\frac{k\tau}{\sqrt{3}}\right){}_1F_2\left(\frac{1}{2};\frac{4}{3},\frac{3}{2};-\frac{1}{12}k^2\tau^2\right)\right) \end{aligned} \tag{34}$$

while for $n = -4/3$ the solution is

$$\begin{aligned} a_k(\tau) &= c_1^k\tau^{2/3}J_{\frac{1}{3}}\left(\frac{k\tau}{\sqrt{3}}\right)+c_2^k\tau^{2/3}Y_{\frac{1}{3}}\left(\frac{k\tau}{\sqrt{3}}\right)\\ &+\frac{\pi k\tau B_k^2}{96\Gamma^2\left(\frac{4}{3}\right)\epsilon_c\sqrt[3]{k\tau}}\\ &\times\left(-2^{2/3}\sqrt[3]{3}\Gamma\left(\frac{1}{3}\right)(k\tau)^{2/3}J_{\frac{1}{3}}\right.\\ &\times\left(\frac{k\tau}{\sqrt{3}}\right){}_1F_2\left(\frac{1}{3};\frac{4}{3},\frac{4}{3};-\frac{1}{12}k^2\tau^2\right)\\ &+2^{2/3}3^{5/6}\Gamma\left(\frac{1}{3}\right)(k\tau)^{2/3}Y_{\frac{1}{3}}\\ &\times\left(\frac{k\tau}{\sqrt{3}}\right){}_1F_2\left(\frac{1}{3};\frac{4}{3},\frac{4}{3};-\frac{1}{12}k^2\tau^2\right)\\ &\times\left.-4\sqrt[3]{2}3^{2/3}\Gamma^2\left(\frac{4}{3}\right)J_{\frac{1}{3}}\left(\frac{k\tau}{\sqrt{3}}\right)G_{1,3}^{2,0}\left(\frac{k^2\tau^2}{12}\middle|\begin{matrix}1\\0,0,\frac{1}{3}\end{matrix}\right)\right). \end{aligned} \tag{35}$$

In the above G_{mn}^{pq} is the Meijer function.

The transverse velocity then takes the form

$$u_\perp(\tau,x_\perp)=\sum_k a_k(\tau)J_1(kx_\perp). \tag{36}$$

In order to completely determine the function $u_\perp(\tau, x_\perp)$ we must fix the integration constants c_1^k and c_2^k. It is convenient to consider the boundary conditions at $\tau \to \infty$. Since $b_\phi^2(\infty, x_\perp) \to 0$ we expect $u_\perp(\infty, x_\perp) \to 0$. By making late-time expansion of $u_\perp$, one finds that $u_\perp$ takes the asymptotic form $f(\tau)\tau^{1/6}$ where $f(\tau)$ is an oscillatory function. In order to prevent divergencies of the transverse velocity one has to impose that the coefficient of $\tau^{1/6}$ is equal to zero. The solutions satisfying these boundary condition at $\tau \to \infty$ are shown in the following.

For $n = -1$,

$$\begin{aligned} c_1^k &= \frac{\sqrt[3]{k}\left(3\pi^{3/2}\Gamma\left(\frac{7}{6}\right)-\sqrt{\pi}\Gamma^2\left(\frac{1}{6}\right)\Gamma\left(\frac{5}{6}\right)\right)B_k^2}{24\sqrt[3]{2}\sqrt[6]{3}\Gamma\left(\frac{5}{6}\right)\Gamma\left(\frac{7}{6}\right)\epsilon_c},\\ c_2^k &= -\frac{\sqrt[3]{\frac{3}{2}}\pi^{3/2}\sqrt[3]{k}B_k^2}{8\Gamma\left(\frac{5}{6}\right)\epsilon_c}. \end{aligned} \tag{37}$$

For $n = -4/3$,

$$c_1^k=\frac{\pi k^{2/3}\Gamma\left(\frac{1}{3}\right)^2B_k^2}{24\,2^{2/3}\sqrt[3]{3}\Gamma\left(\frac{4}{3}\right)\epsilon_c},\ c_2^k=-\frac{\pi k^{2/3}\Gamma\left(\frac{1}{3}\right)^2B_k^2}{8\,2^{2/3}3^{5/6}\Gamma\left(\frac{4}{3}\right)\epsilon_c}. \tag{38}$$

After obtaining $u_\perp(\tau, x_\perp)$ we can get, correspondingly, the modified energy density from Eq. (18). For $n = -1$, it reads:

$$\begin{aligned} \epsilon_1(\tau,x_\perp) &= \sum_k h_k(\tau)+\sum_k\frac{1}{24k\tau^{7/3}}\\ &\left(32\epsilon_c[J_0(kx_\perp)-1][a_k(\tau)-3ta_k'(\tau)]\right.\\ &-9B_k^2k\tau^{4/3}\left[k^2x_\perp^2\,{}_0F_1\left(2;-\frac{1}{4}k^2x_\perp^2\right)\right.\\ &\left.\left.+2kx_\perp J_1(kx_\perp)-8J_0(kx_\perp)+8\right]\right), \end{aligned} \tag{39}$$

where $h(\tau)$ is the constant of integration and can be obtained form Eq. (17). We find,

$$h_k(\tau)=\frac{\int_1^\tau\frac{4}{3}k\epsilon_ca_k(s)\,ds}{\tau^{4/3}}. \tag{40}$$

For $n = -4/3$, instead,

$$\begin{aligned} \epsilon_1(\tau,x_\perp) &= \sum_k h_k(\tau)+\sum_k\frac{1}{6k\tau^{7/3}}(8\epsilon_c[J_0(kx_\perp)-1](a_k(\tau)\\ &-3ta_k'(\tau))-27B_k^2k\tau\left[-G_{1,3}^{2,0}\left(\frac{k^2x_\perp^2}{4}\middle|\begin{matrix}1\\0,0,0\end{matrix}\right)\right.\\ &\left.+J_0(kx_\perp)-1\right]\Big), \end{aligned} \tag{41}$$

where

$$h_k(\tau)=\frac{\int_1^\tau\left(\frac{4}{3}k\epsilon_ca_k(s)-\frac{B_k^2}{s}\right)ds}{\tau^{4/3}}. \tag{42}$$

Note that, the integrals (40) and (42) should be calculated numerically.

4 Results and discussion

In this section we will present the transverse velocity and energy density numerically obtained from our perturbation approach: this two quantities will help in understanding the space time evolution of the quark-gluon plasma in heavy ion collisions. The typical magnetic field produced in Au–Au peripheral collisions at $\sqrt{s_{NN}} = 200$ GeV reaches $|eB| \sim 10m_\pi^2$. The estimate $\epsilon \sim 5.4$ GeV/fm^3 at a proper time of about $\tau = 1$ fm is taken from [2]. By taking $m_\pi \approx 150$ MeV and $e^2 = 4\pi/137$, one finds $B^2/\epsilon_c \sim 0.6$. This value in central collisions is much smaller than in peripheral collisions; therefore, in our calculations we assumed the even smaller value $B_c^2/\epsilon_c = 0.1$, which correspond to $\sigma \sim 0.015$. Note that in our calculations any change in the ratio B_c^2/ϵ_c will only scale the solutions. We will use cylindrical coordinates whose longitudinal component is chosen to be the third component of Cartesian coordinate, e.g., $\vec{x} = (x_\perp, \phi, z)$.

4.1 Numerical solution for the case $n = -1$

The external magnetic field profile Eq. (21) can be reproduced by expressing b_ϕ^2 via a series of Bessel functions as shown in Eq. (29). The first ten coefficients of series and on the B_k^2 calculated according to Eq. (30) for $\alpha = 0.1$ are: $B_c^2\{0.112499,\ 0.111212,\ 0.0707575,\ 0.0391739,\ 0.0231679,\ 0.0153799,\ 0.0110821,\ 0.0084056,\ 0.00661182,\ 0.00534074\}$. In order to reproduce the assumed external magnetic profile Eq. (21) we had to take in the calculation the first 100 terms of the series. Figure 2 shows a comparison between the approximated magnetic field in Bessel series and the assumed magnetic profile Eq. (21). Note that the Fourier expansion matches the assumed magnetic profile in the whole region of $x_\perp$, hence the solutions for the radial velocity and the energy density are valid in the entire region $x_\perp \in (0, \infty)$.

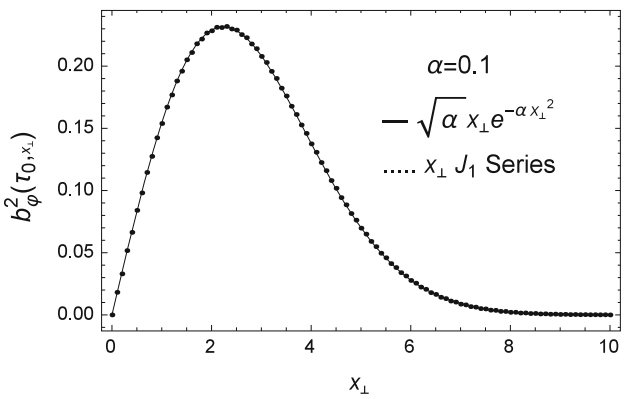

Fig. 2 A comparison between the approximated b_ϕ^2 in Bessel series (dotted curve) and the assumed external magnetic field (solid curve) with $n = -1$

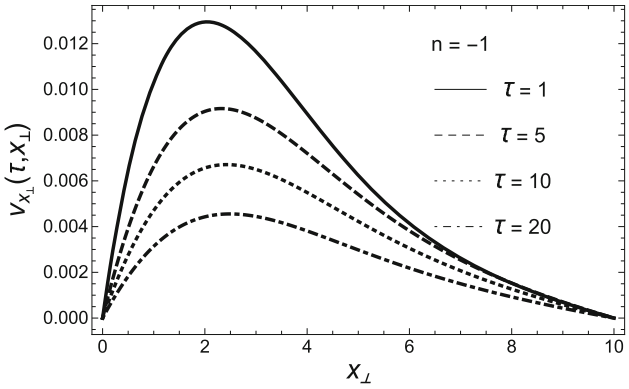

Fig. 3 $v_{x_\perp}$ as a function of $x_\perp$ for different values of τ

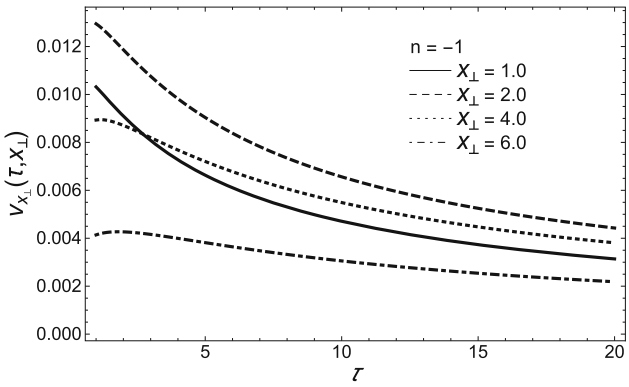

Fig. 4 $v_{x_\perp}$ as a function of τ for different values of $x_\perp$

Next we show plots of the fluid velocity ($v_{x_\perp} \equiv u_\perp/u_\tau$) and of the energy density modified by the magnetic field with $B_c^2/\epsilon_c = 0.1$. In Figs.3 and 4 $v_{x_\perp}(\tau, x_\perp)$ is displayed, at either fixed τ or fixed $x_\perp$, respectively. From Fig.3, one finds that $v_{x_\perp}(\tau, 0) = 0$ and the radial velocity $v_{x_\perp}$ first increases from $x_\perp = 0$, has a maximum at intermediate $x_\perp$ and then gradually decreases with $x_\perp$. As shown in Fig.4, $v_{x_\perp}$ at fixed $x_\perp$ becomes smaller at late times, due to the decay of the magnetic field, in agreement with the curves displayed in Fig.3.

Figure 5 shows the correction energy density $\epsilon_1(\tau, x_\perp)$ as a function of $x_\perp$ for different values of τ; we remind the reader that the total energy density is $\epsilon = \epsilon_0(\tau) + \epsilon_1(\tau, x_\perp)$ and the latter is the component which is truly affected by the magnetic field. Figure 6 shows the correction energy density as a function of τ for different values of $x_\perp$. Here we find that for $x_\perp = 0$ the correction energy density is positive, starting from zero at proper time $\tau = 1$ fm and showing a shallow maximum; for $x_\perp = 0.5$ fm the correction energy density is negative at $\tau = 1$ fm and increases with τ reaching zero at approximately $\tau = 4.5$ fm, becoming then slightly positive. For the other values of $x_\perp$ the correction energy density is negative at any time and monotonically increases toward zero.

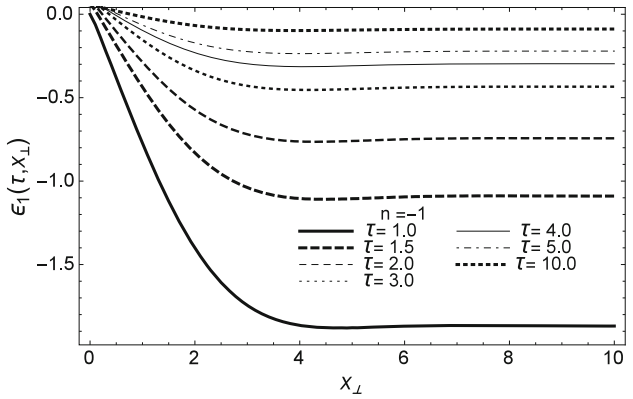

Fig. 5 ϵ_1 as a function of $x_\perp$ for different values of τ

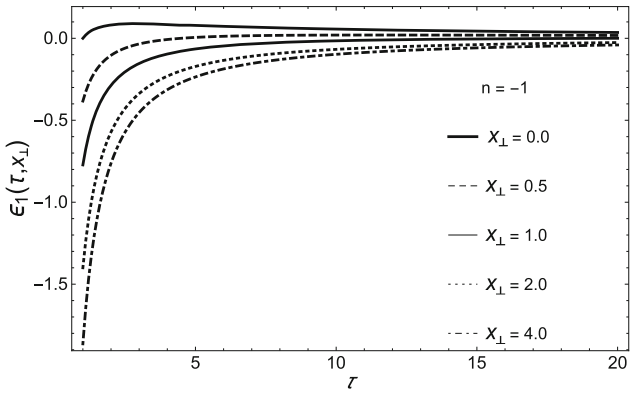

Fig. 6 ϵ_1 as a function of τ for different values of $x_\perp$

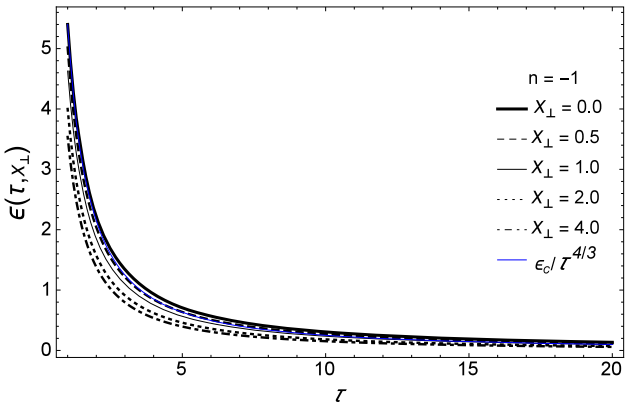

Fig. 7 $\epsilon(\tau, x_\perp)$ as a function of τ for several values of $x_\perp$

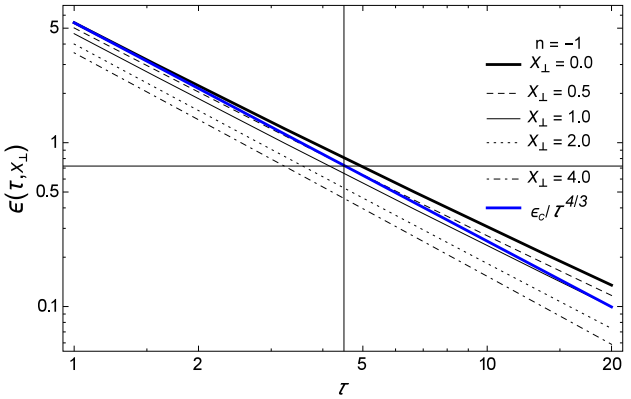

Fig. 8 Log–Log plot of $\epsilon(\tau, x_\perp)$ as a function of τ for several values of $x_\perp$. The bold blue line shows the dependence $\epsilon/\tau^{4/3}$, where ϵ is in GeV/fm^3 and τ in fm. We have chosen $\epsilon = 5.4$ GeV/fm^3 at $\tau = 1$ fm from [2]

This behavior can also be seen in Figs.7 and 8 which show the normal and Log-Log plots of the total energy density $\epsilon(\tau, x_\perp)$ as a function of τ for several values of $x_\perp$, respectively. The time evolution of the energy density for different values of $x_\perp$ in the work of Gubser [2] has nearly the same behavior as in Fig. 8, stemming from a similar trend of the correction energy density as a function of τ, like the one illustrated in our Fig. 6. In the Gubser work for $\tau < 4.6$ fm the energy density is positive for $x_\perp \leq 3$ fm and negative for $x_\perp \geq 4$ fm and it is negative for any $x_\perp$ for $\tau > 4.6$ fm.

It is interesting to investigate variations of the spatial width of the external magnetic field: this affects the Fourier series which reproduces the assumed distribution for the magnetic field; moreover we find that $v_{x_\perp}(\tau, x_\perp)$ and $\epsilon_1(\tau, x_\perp)$ have an important dependence on the parameter α (with dimension square of inverse length), which characterizes the spatial width of the magnetic field. In Fig. 9, we plot the external magnetic profile at $\tau = 1$ fm for several different values of α. In Figs. 10 and 11, we plot $v_{x_\perp}$ and ϵ_1 at $\tau = 1$ fm for references. The $v_{x_\perp}$ gets smaller when α is increased. It seems that the parameter α plays the role of

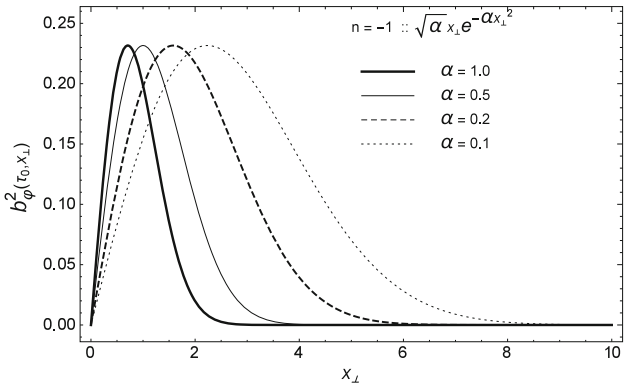

Fig. 9 $b_\phi^2(\tau, x_\perp)$ as a function of $x_\perp$ for different values of α at $\tau_0 = 1$ fm

the parameter $1/q^2$ in Ref. [2]: indeed the radial flow velocity (versus $x_\perp$ at $\tau = 0.6$ fm) becomes smaller when $1/q$ increases.

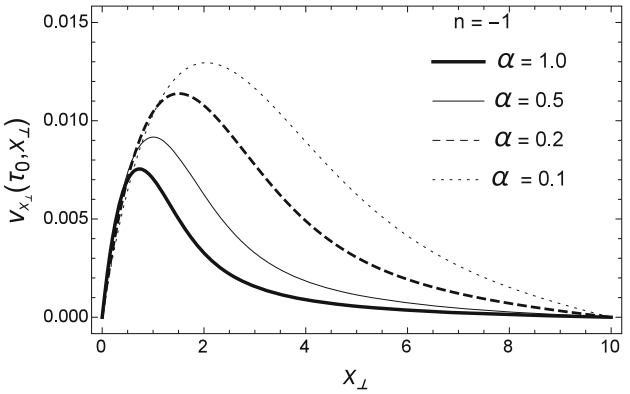

Fig. 10 $v_{x_\perp}(\tau, x_\perp)$ as a function of $x_\perp$ for different values of α at $\tau_0 = 1$ fm

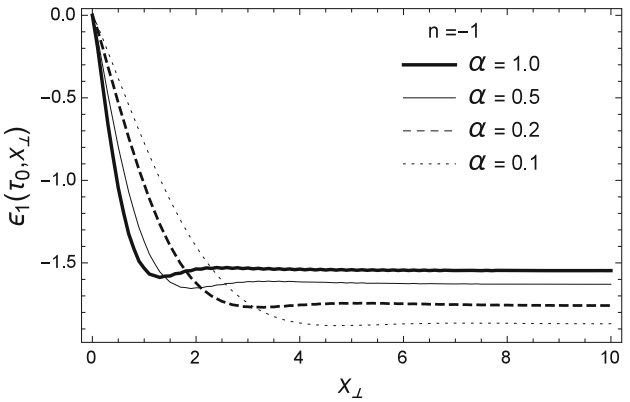

Fig. 11 $\epsilon_1(\tau, x_\perp)$ as a function of $x_\perp$ for different values of α at $\tau_0 = 1$ fm

4.2 Numerical solution for the case $n = -4/3$

For the case $n = -4/3$, the external magnetic field profile Eq. (21) can be reproduced as a series of Bessel functions as shown in Eq. (31). The first 10 coefficients B_k^2 calculated according to of Eq. (32) for $\alpha = 0.1$ are: $B_c^2\{0.04745, 0.0371507, -0.00832931, -0.0215885, -0.0146208, -0.00825935, -0.00515007, -0.00362071, -0.00269932, -0.00212629\}$. In order to reproduce the assumed external magnetic profile Eq. (21), one may take the first 100 terms of the series in the calculation. Fig. 12 shows a comparison between the approximated magnetic field by the Bessel series and the assumed magnetic profile Eq. (21). Figures 13 and 14 show $v_{x_\perp}(\tau, x_\perp)$ at either fixed τ or fixed $x_\perp$, respectively. The qualitative behaviors of $v_{x_\perp}(\tau, x_\perp)$ in both figures are different from the case $n = -1$ and the amplitude is smaller. While for $n = -1$, the direction of the fluid velocity is always positive, for $n = -4/3$ the direction of fluid velocity changes during the expansion of the fluid.

Figure 15 shows the correction energy density as a function of $x_\perp$ for different values of τ. Figure 16 shows the correction energy density as a function of τ for different values of $x_\perp$. Figures 17 and 18 show the normal and Log-Log plots of the total $\epsilon(\tau, x_\perp)$ as a function of τ for several values of $x_\perp$, respectively. In Fig. 15, we find that for $x_\perp = 0$ the correction energy density is always positive and then it decreases from the value at $x_\perp = 0$ with increasing $x_\perp$. From Fig. 16 one also finds that for the case $n = -4/3$ the correction energy density is always positive, at variance with the

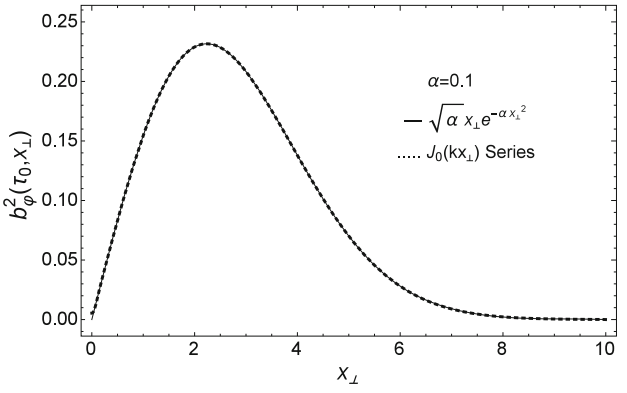

Fig. 12 A comparison between the approximated b_ϕ^2 in Bessel series (dotted curve) and the assumed external magnetic field (solid curve) with $n = -4/3$

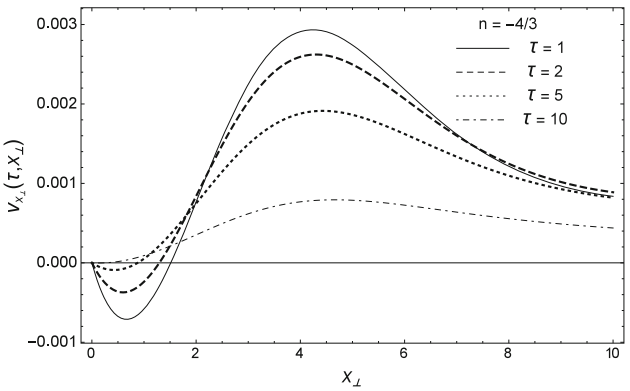

Fig. 13 $v_{x_\perp}$ as a function of $x_\perp$ for different values of τ

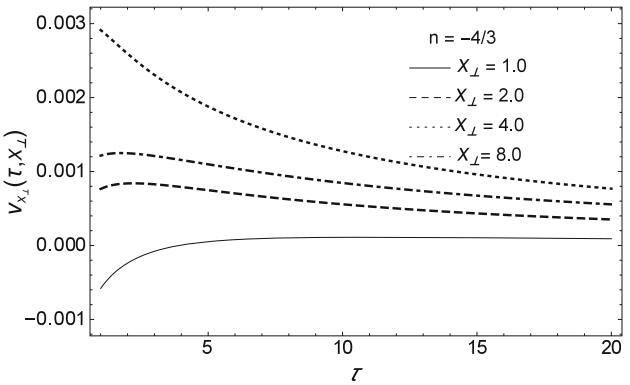

Fig. 14 $v_{x_\perp}$ as a function of τ for different values of $x_\perp$

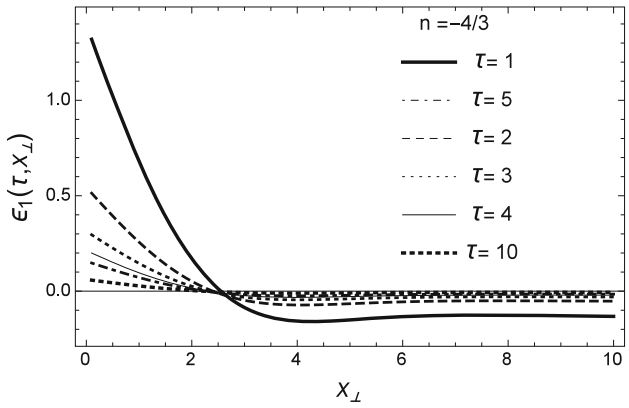

Fig. 15 ϵ_1 as a function of $x_\perp$ for different values of τ

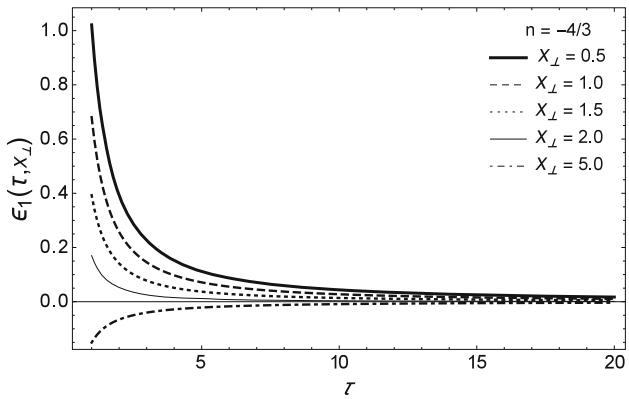

Fig. 16 ϵ_1 as a function of τ for different values of $x_\perp$

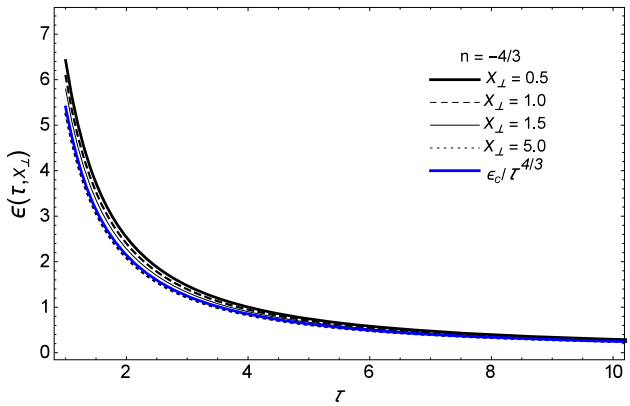

Fig. 17 $\epsilon(\tau, x_\perp)$ as a function of τ for several values of $x_\perp$

case $n = -1$. The same feature can be obviously extracted from Figs. 17 and 18.

Also for the case $n = -4/3$, we plot the external magnetic profile at $\tau = 1$ fm for several different values of α in Fig. 19. In Figs. 20 and 21, we plot $v_{x_\perp}$ and ϵ_1 at $\tau = 1$ fm. The qualitative behavior of $v_{x_\perp}$ and ϵ_1 are similar to the case $n = -1$.

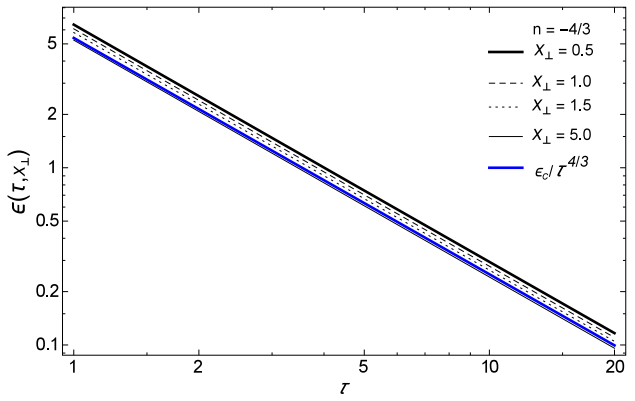

Fig. 18 Log-Log plot of $\epsilon(\tau, x_\perp)$ as a function of τ for several values of $x_\perp$. The bold blue line shows the dependence $\epsilon/\tau^{4/3}$, where ϵ is in GeV/fm^3 and τ in fm. We have chosen $\epsilon = 5.4$ GeV/fm^3 at $\tau = 1$ fm from [2]

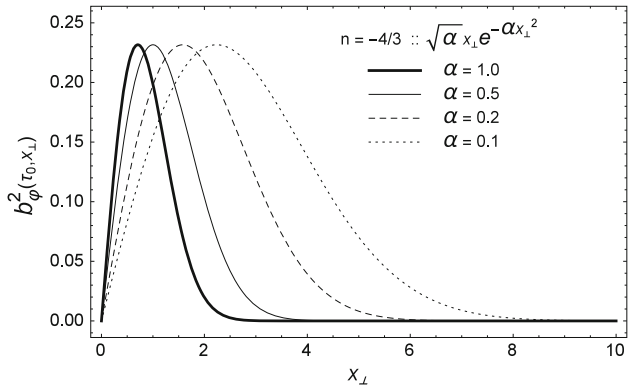

Fig. 19 $b_\phi^2(\tau, x_\perp)$ as a function of $x_\perp$ for different values of α at $\tau_0 = 1$ fm

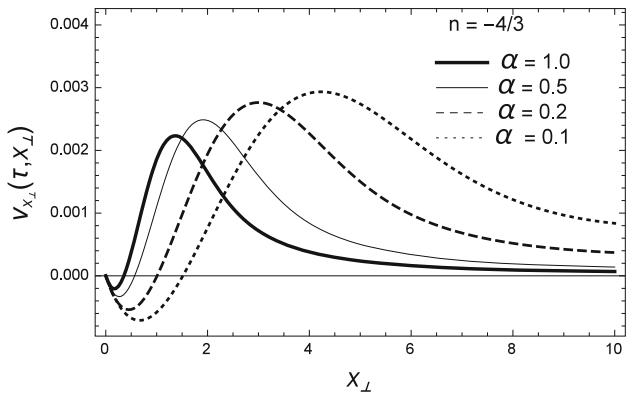

Fig. 20 $v_{x_\perp}(\tau, x_\perp)$ as a function of $x_\perp$ for different values of α at $\tau_0 = 1$ fm

5 Transverse momentum spectrum in the presence of a weak external magnetic field

In the previous sections we have obtained as analytical solution the transverse velocity and energy density in the presence of a weak magnetic field. Now we can use these results to

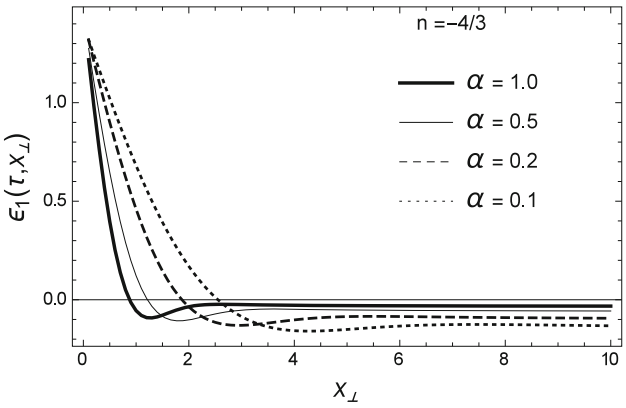

Fig. 21 $\epsilon_1(\tau, x_\perp)$ as a function of $x_\perp$ for different values of α at $\tau_0 = 1$ fm

estimate the transverse momentum spectrum emerging from the Magneto-hydrodynamic solutions.

From the local equilibrium hadron distribution the transverse spectrum is calculated at the freeze out surface via the Cooper–Frye (CF) formula:

$$S = E\frac{d^3N}{dp^3} = \frac{dN}{p_T dp_T dy d\varphi} = \int d\Sigma_\mu p^\mu \exp\left(\frac{-p^\mu u_\mu}{T_f}\right) \tag{43}$$

We note that T_f is the temperature at the freeze out surface. The latter is the isothermal surface in space-time at which the temperature of inviscid fluid is related to the energy density as $T \propto \epsilon^{1/4}$. It must satisfy $T(\tau, x_\perp) = T_f$.

In our convention,

$$\begin{aligned} d\Sigma_\mu &= (-1, R_f, 0, 0)\tau_f x_\perp dx_\perp d\varphi d\eta, \qquad (44)\\ p^\mu &= (m_T \cosh(Y-\eta),\, P_T \cos(\varphi_p - \varphi),\\ &\quad r p_T \cos(\varphi_p - \varphi),\, \tau_f m_T \sinh(Y-\eta)), \end{aligned}$$

$$\begin{aligned} d\Sigma_\mu p^\mu &= [-m_T \cosh(Y-\eta)\\ &\quad + p_T R_f \cos(\varphi_p - \varphi)]\tau_f x_\perp dx_\perp d\varphi d\eta, \qquad (45)\\ p^\mu u_\mu &= -m_T \cosh(Y-\eta)u_\tau + p_T \cos(\varphi_p - \varphi)u_\perp, \qquad (46) \end{aligned}$$

where $R_f \equiv -\frac{\partial\tau}{\partial x_\perp} = \frac{\partial_\perp T}{\partial_\tau T}\,|_{T_f}$. Here $\tau = \sqrt{t^2 - z^2}$ is the longitudinal proper time, $x_\perp$ the transverse (cylindrical) radius, $\eta = \frac{1}{2}\log\frac{t+z}{t-z}$ the longitudinal rapidity (hyperbolic arc angle), the azimuthal angle φ_p belonging to the spacetime point x^μ . Similarly $u_\perp$ is the transverse flow velocity and φ is its asimuthal angle. Finally p_T is the detected transverse momentum, $m_T = \sqrt{m^2 + p_T^2}$ the corresponding transverse mass, while Y is the observed longitudinal rapidity, which gives our final expression for the CF formula

$$\begin{aligned} S &= \frac{g_i}{2\pi^2}\int_0^{x_f} x_\perp\, \tau_f(x_\perp)\, dx_\perp\\ &\quad \times \left[m_T K_1\left(\frac{m_T u_\tau}{T_f}\right) I_0\left(\frac{m_T u_\perp}{T_f}\right)\right.\\ &\quad \left. + p_T R_f K_0\left(\frac{m_T u_\tau}{T_f}\right) I_1\left(\frac{m_T u_\perp}{T_f}\right)\right] \qquad (47) \end{aligned}$$

Where $\tau_f(x_\perp)$ is the solution of the $T(\tau_f, x_\perp) = T_f$ and the degeneracy is $g_i = 2$ for both the pions and the protons. The above integral over $x_\perp$ on the freeze-out surface is evaluated numerically.

The spectrum Eq. (47) is illustrated in Figs. 22 and 23 for three different values of the freeze out temperature (140, 150 and 160 MeV) and compared with experimental results obtained at PHENIX [33] in central collisions. Our proton spectrum appear to underestimate the experimental data, except at low p_T, but their behavior with $p_T$has the correct trend of a monotonical decrease. The pion spectrum, instead, appears in fair agreement with the experimental results, which are very close to the theoretical curves. This is an indication that hadrons with different masses have dif-

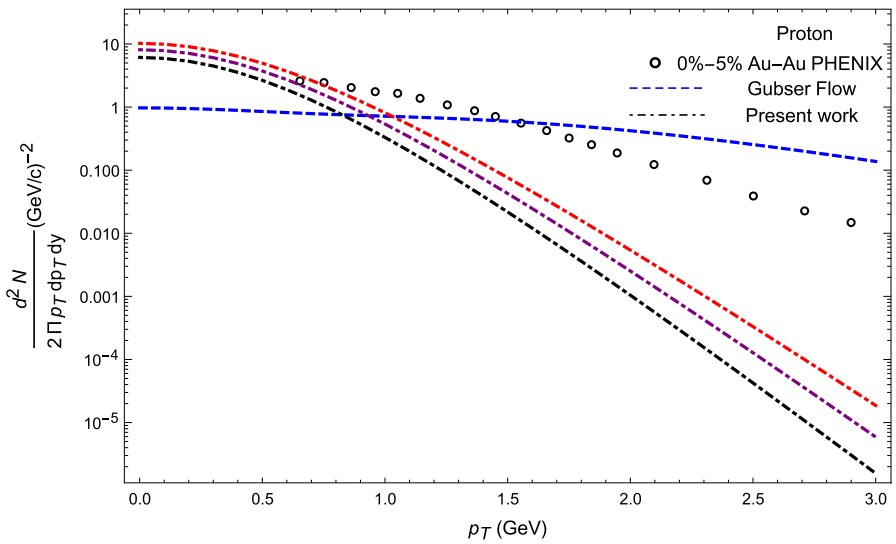

Fig. 22 Proton transverse spectrum from central Au-Au collisions: black, purple and red lines correspond to a freeze out temperature of 140, 150 and 160 MeV, respectively. Circles: PHENIX data [33]

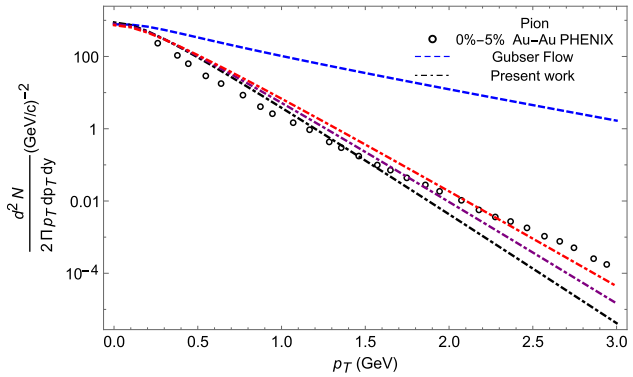

Fig. 23 Pion transverse spectrum from central Au-Au collisions: black, purple and red lines correspond to a freeze out temperature of 140, 150 and 160 MeV, respectively. Circles: PHENIX data [33]

ferent sensitivities to the underlying hydrodynamic flow and to the electromagnetic fields. Indeed, the difference between the charge-dependent flow of light pions and heavy protons might arise because the former are more affected by the weak magnetic field than the heavy protons [34].

For comparison, we also show the results obtained by Gubser, which appear to be more flat and typically overestimate the experiment. We also notice that, for the proton case, the highest value of the freeze out temperature we employed (as suggested, e.g. in Ref. [35]) slightly brings (for protons) the calculation closer to the experimental data; however it also shows a kind of saturation phenomenon and points to the need of including other effects not considered in the present work.

6 Conclusions

In the present work, we investigated central heavy ion collisions in the presence of a transverse external magnetic field. Making use of Milne coordinates, in our setup the medium is boost-invariant along the z direction and the magnetic field, which is a function of τ and $x_\perp$, points along the ϕ direction. The energy conservation and Euler equations reduced to two coupled differential equations, which we solved analytically in the weak-field approximation. We showed in detail how the fluid velocity and energy density are modified by the magnetic field. The solutions obtained by our numerical calculations assume an initial energy density of the fluid at time $\tau = 1$ fm fixed to ~ 5.4 GeV/fm^3 and a ratio of the magnetic field energy to the fluid energy density, σ, fixed to ~ 0.015. We consider two different decays with time of the magnetic field: τ^n, with $n = -1$ or $n = -4/3$. A visual presentation of the flow for $n = -1$ can be find in Figs. 3 and 4 and for $n = -4/3$ in Figs. 13 and 14.

We remark that in Ref. [4] the external magnetic field was approximated by a Fourier cosine series and, due to the oscillatory behavior of the cosine function, the magnetic field reduces to zero in the fringes for $|x| = \pi$. Consequently, these authors had to focus on the valid region $-\pi < x < \pi$ and the behavior of the transverse velocity and of the correction energy density was difficult to analyze near the fringes. In the present work the magnetic field is approximated by a series of Bessel functions and the solutions are valid for the entire region of $x_\perp$, i.e., $(0, \infty)$.

Another point concerning the choice of the τ dependence of the magnetic field is related to the ratio σ between magnetic and fluid energy densities: in Ref. [3], it was found that in central collisions, at the center of the collision region, $\sigma \ll 1$ for most of the events; nevertheless, large values of σ were observed in the outer regions of the collision zone. Therefore, our assumption for the spatial distribution of the external magnetic field for the case $n = -1$ may be more realistic at face of the physical conditions.

In general, our study in a simple setup, which includes an azimuthal magnetic field in the matter distribution, is worthwhile to check the possible effect of this change on the transverse expansion of the fluid. We showed that by combining the azimuthal magnetic field with the boost symmetry along the beam direction, a radial flow perpendicular to the beam axis is created and the energy density of the fluid is altered. We stress that the present work presents an approximated calculation which can be useful for cross checking current and future numerical calculations in some limiting region. Indeed, the effect of such a scenario on hadronic flow in heavy ion collisions requires more pragmatic debates.

Our study can be generalized in many directions: breaking of rotational symmetry can be introduced, the conservation equation can be coupled to Maxwell's equations and solved consistently. Of course in this case only numerical solutions can be found, while in the present paper we were able to obtain analytical solutions.

Data Availability Statement This manuscript has no associated data or the data will not be deposited. [Authors' comment: Data will be sent by the authors upon request to anybody interested.]

Funded by SCOAP^3.

References

1. J.D. Bjorken, Phys. Rev. D **27**, 140 (1983)
2. S.S. Gubser, Symmetry constraints on generalizations of Bjorken flow. Phys. Rev. D **82**, 085027 (2010)

3. V. Roy, P. Shi, Event-by-event distribution of magnetic field energy over initial fluid energy density in $\sqrt{S_{NN}} = 200$ GeV Au-Au collisions. Phys. Rev C **92**, 064902 (2015)
4. P. Shi, D.-L. Yang, Transverse flow induced by inhomogeneous magnetic fields in the Bjorken expansion. Phys. Rev. D **93**, 054042 (2016)
5. K. Tuchin, Time and space dependence of the electromagnetic field in relativistic heavy-ion collisions. Phys. Rev. C **88**(2), 024911 (2013)
6. K. Tuchin, Particle production in strong electromagnetic fields in relativistic heavy-ion collisions. Adv. High Energy Phys. **2013**, 490495 (2013)
7. K. Tuchin, Electromagnetic fields in high energy heavy-ion collisions. Int. J. Mod. Phys. E **23**(1), 1430001 (2014)
8. B.G. Zakharov, Electromagnetic response of quark gluon plasma in heavy ion collisions. Phys. Lett. B **737**, 262–266 (2014)
9. L. McLerran, V. Skokov, Comments About the Electromagnetic Field in Heavy-Ion Collisions. Nucl. Phys. A **929**, 184 (2014)
10. W.T. Deng, X.G. Huang, Event-by-event generation of electromagnetic fields in heavy-ion collisions. Phys. Rev. C **85**, 044907 (2012)
11. H. Li, X.-L. Sheng, Q. Wang, Electromagnetic fields with electric and chiral magnetic conductivities in heavy ion collisions. Phys. Rev. C **94**, 044903 (2016)
12. U. Gursoy, D. Kharzeev, K. Rajagopal, Magnetohydrodynamics, charged currents and directed flow in heavy ion collisions. Phys. Rev. C **89**(5), 054905 (2014)
13. A. Bzdak, V. Skokov, Event-by-event fluctuations of magnetic and electric fields in heavy ion collisions. Phys. Lett. B **710**, 171 (2012)
14. V.V. Skokov, A.Y. Illarionov, V.D. Toneev, Estimate of the magnetic field strength in heavy-ion collision. Int. J. Mod. Phys. A **24**(31), 5925–5932 (2009)
15. Yang Z, Chun-Bin Y, Xu C, Sheng-Qin F, A Systematic study of magnetic field in relativistic heavy-ion collisions in the RHIC and LHC energy regions. Adv High Energy Phys 2014, Article ID 193039 (2014)
16. V. Voronyuk, V.D. Toneev, W. Cassing, E.L. Bratkovskaya, V.P. Konchakovski, S.A. Voloshin, Electromagnetic field evolution in relativistic heavy-ion collisions. Phys. Rev C **83**, 054911 (2011)
17. D.E. Kharzeev, L.D. McLerran, H.J. Warringa, The effects of topological charge change in heavy ion collisions: event by event P and CP violation. Nucl. Phys. A **803**, 227 (2008). arXiv:0711.0950 [hep-ph]
18. D.E. Kharzeev, Topologically induced local P and CP violation in QCD x QED. Ann. Phys. **325**, 205 (2010). arXiv:0911.3715 [hep-ph]
19. D.E. Kharzeev, H.-U. Yee, Chiral magnetic wave. Phys. Rev. D **83**, 085007 (2011). arXiv:1012.6026 [hep-th]
20. Y. Burnier, D.E. Kharzeev, J. Liao, H.-U. Yee, Chiral magnetic wave at finite baryon density and the electric quadrupole moment of quark-gluon plasma in heavy ion collisions. Phys. Rev. Lett. **107**, 052303 (2011). arXiv:1103.1307 [hep-ph]
21. V. Roy, S. Pu, L. Rezzolla, D. Rischke, Analytic Bjorken flow in one-dimensional relativistic magnetohydrodynamics. Phys. Lett. B **750**, 42–50 (2015)
22. S. Pu, V. Roy, L. Rezzolla, D.H. Rischke, Bjorken flow in one-dimensional relativistic magnetohydrodynamics with magnetization. Phys. Rev. D **93**, 074022 (2016)
23. L.G. Pang, G. Endrődi, H. Petersen, Magnetic field-induced squeezing effect at RHIC and at the LHC. Phys. Rev. C **93**, 044919 (2016)
24. G. Inghirami, L. Del Zanna, A. Beraudo, M. Haddadi Moghaddam, F. Becattini, M. Bleicher, Numerical magneto-hydrodynamics for relativistic nuclear collisions. Eur. Phys. J. C **76**, 659 (2016)
25. M.H. Moghaddam, B. Azadegan, A.F. Kord, W.M. Alberico, Non-relativistic approximate numerical ideal-magneto-hydrodynamics of (1+1D) transverse flow in Bjorken scenario. Eur. Phys. J. C **78**, 255 (2018)
26. A. Das, S.S. Dave, P.S. Saumia, A.M. Srivastava, Effects of magnetic field on the plasma evolution in relativistic heavy-ion collisions. Phys. Rev. C **96**, 034902 (2017)
27. V. Roy, S. Pu, L. Rezzolla, D.H. Rischke, Effects of intense magnetic fields on reduced-MHD evolution in $\sqrt{s_{NN}} = 200$ GeV Au+Au collisions. Phys. Rev. C **96**, 054909 (2017)
28. B. Feng, Z. Wang, Effect of an electromagnetic field on the spectra and elliptic flow of particles. Phys. Rev. C **95**, 054912 (2017)
29. M. Greif, C. Greiner, Z. Xu, Magnetic field influence on the early time dynamics of heavy-ion collisions. Phys. Rev. C **96**, 014903 (2017)
30. K. Hattori, X.-G. Huang, D. Satow, D.H. Rischke, Bulk viscosity of quark-gluon plasma in strong magnetic fields. Phys. Rev. D **96**, 094009 (2017)
31. J. Goedbloed, R. Keppens, S. Poedts, *Advanced Magnetohydrodynamics with Applications to Laboratory and Astrophysical Plasmas* (Cambridge University Press, Cambridge, 2010)
32. A.M. Anile, *RelativistiC Fluids and Magneto-fluids* (Cambdridge University Press, Cambridge, 1989)
33. K. Adcox et al., (PHENIX Collaboration), Formation of dense partonic matter in relativistic nucleusnucleus collisions at RHIC: Experimental evaluation by the PHENIX Collaboration. Nucl. Phys. A **757**, 184 (2005)
34. U. Gursoy, D. Kharzeev. E. Marcus, K. Rajagopal and C. Shen, Charge dependent flow induced by magnetic and electric field in heavy ion collisions. Phys. Rev. C **98**, 055201 (2018).
35. C. Ratti, R. Bellwied, J. Noronha-Hostler, P. Parotto, I. Portillo Vazquez, J.M. Stafford. arXiv:1805.00088 [hep-ph]